Available online at www.sciencedirect.com
ScienceDirect
Journal of Nuclear Materials 362 (2007) 1–13
journal of nuclear materials
www.elsevier.com/locate/jnucmat

The impact of radiolytic yield on the calculated ECP in PWR primary coolant circuits

Mirna Urquidi-Macdonald [a,*], Jonathan Pitt [a], Digby D. Macdonald [b]

[a] Department of Engineering Science and Mechanics, Pennsylvania State University, 212 EES Building, University Park, PA 16802, USA
[b] Center for Electrochemical Science and Technology, Pennsylvania State University, 201 Steidle Building, University Park, PA 16802, USA

Received 4 April 2006

Abstract

A code, PWR–ECP, comprising chemistry, radiolysis, and mixed potential models has been developed to calculate radiolytic species concentrations and the corrosion potential of structural components at closely spaced points around the primary coolant circuits of pressurized water reactors (PWRs). The pH(T) of the coolant is calculated at each point of the primary-loop using a chemistry model for the $B(OH)_3 + LiOH$ system. Although the chemistry/radiolysis/mixed potential code has the ability to calculate the transient reactor response, only the reactor steady state condition (normal operation) is discussed in this paper. The radiolysis model is a modified version of the code previously developed by Macdonald and coworkers to model the radiochemistry and corrosion properties of boiling water reactor primary coolant circuits. In the present work, the PWR–ECP code is used to explore the sensitivity of the calculated electrochemical corrosion potential (ECP) to the set of radiolytic yield data adopted; in this case, one set had been developed from ambient temperature experiments and another set reported elevated temperatures data. The calculations show that the calculated ECP is sensitive to the adopted values for the radiolytic yields.
© 2006 Elsevier B.V. All rights reserved.

1. Background

Sophisticated radiolysis/chemical/electrochemical codes have been developed for describing the electrochemistry and corrosion properties of the primary coolant circuits of boiling water reactors (BWRs) [1–14]. Some of the component models of these codes are routinely used to calculate radiolytic species concentrations, electrochemical corrosion potential (ECP), crack growth rate, and accumulated damage over the full range of operating conditions experienced in this type of reactor [9–14]. The impetus for developing the models was to prevent, or at least minimize, intergranular stress corrosion cracking (IGSCC) and irradiation assisted stress corrosion cracking (IASCC) of stainless steels components in the reactor primary coolant circuits. Extensive experimental and theoretical work over the past thirty years on IGSCC of sensitized Type 304 SS has shown that the crack growth rate can be significantly reduced, or even eliminated, by

* Corresponding author. Tel.: +1 814 863 4217; fax: +1 814 863 7967.
E-mail addresses: mumesm@engr.psu.edu (M. Urquidi-Macdonald), ddm2@psu.edu (D.D. Macdonald).

0022-3115/$ - see front matter © 2006 Elsevier B.V. All rights reserved.
doi:10.1016/j.jnucmat.2006.10.012

Nomenclature

a, b, and c constants in terms of fundamental parameters
a_R and a_O thermodynamic activities
b_a and b_c anodic and cathodic Tafel constants, 1/V
b_f and b_r forward and reverse Tafel constants, 1/V
C_m, and C_s concentrations of species m and s, mol/cm^3
$C^b_{O/R}$ bulk concentration of O or R, mol/cm^3
D_i diffusivity of the redox species i, cm^2/s
d channel diameter, cm
ECP electrochemical potential, V
E_a activation energy (Table 1)
E applied or spontaneous potential, V
$E^0_{R/O}$ standard potential, V
$E^e_{R/O}$ equilibrium potential, V
E_o empirical constant that is derived from the polarization curve for the oxidation of the steel
$\widetilde{F}$ A conversion factor equal to 6.25×10^{13} (from R/s to eV/g s)
f_{H_2} partial pressure of hydrogen
F Faraday's constant
G^n, G^g, and G^α radiolytic yields for neutrons, gamma photons, and alpha particles, respectively, in number of particles per 100 eV of energy absorbed
$i_{R/O,j}$ current density due to the jth redox couple, A/cm^3
$i_{i,R/O}$ limiting currents, A/cm^3
$i_{0,R/O}$ exchange current density, A/cm^3
i_{corr} corrosion current density, A/cm^3
k_0 rate constant at temperature T_0 (room temperature), K
k_j rate constant for the reaction between two different species
M number of species ($M = 14$)
N number of reactions in the model (i.e., $N = 34$ (from Table 1))
N_v Avogadro's number
$\overline{N}_i$ vector flux of each dissolved species i
n electron number for the half cell reaction
R universal gas constant
R^c_i rate of change for each species i, at a given location c, mol/cm^3 s
R_i species total rate formed by the effect of radiolysis, mol/cm^3 s
R^y_i species radiolytic rate of production, mol/cm^3 s
Re Reynolds number ($Re = Vd/\eta$)
pH_T pH at the operating Kelvin temperature (T)
Sc Schmidt number ($Sc = \eta/D_i$)
T temperature, K
V average flow velocity, cm/s
$\overline{V}$ velocity vector for each considered section, cm/s
z_i charge number (with sign) on the ion i
$\overline{\nabla} C_i$ gradient of the concentration of species i, mol/cm^2
$\overline{\nabla}\phi$ electrical field strength, V/cm
$\overline{\nabla}$ space derivative vector, 1/cm
Γ^γ, Γ^n, and Γ^α gamma photon, neutron, and alpha particle energy dose rates, respectively, R/s
η kinematics' viscosity
ρ water density, g/cm^3

displacing the electrochemical corrosion potential (ECP) in the negative direction [15–18]. Thus, based upon in-reactor measurements [19], displacement of the ECP to a value that is more negative than $-0.230 V_{SHE}$ at 288 °C in pure water results in the cessation of IGSCC, and the crack then propagates by creep alone at a rate that does not pose a threat to coolant circuit integrity.

The currently preferred method of displacing the ECP in the negative direction in a BWR is by adding a small amount of hydrogen to the reactor feed water [15–18]. The technique, invented in Sweden, but which has been most extensively implemented in the US, is termed 'Hydrogen Water Chemistry (HWC)', in which small amounts of hydrogen (0.5–2 ppm) are added to the feedwater, in order to displace the ECP in the negative direction from that observed under 'Normal Water Chemistry (NWC)', in which no hydrogen is added to the coolant. HWC has now been implemented in many BWRs in the US and elsewhere, and it is generally found to be effective in out-of-core regions of the primary heat transport circuit where boiling does not occur. However, it is deemed to be much less

effective in boiling in-vessel regions, because the hydrogen is stripped from the coolant.

Macdonald et al. [2] calculated H_2, O_2, and H_2O_2 concentrations at closely-spaced points around the primary heat transport circuits of various GE-designed BWRs, and then estimated the ECP using a mixed potential model (MPM) as a function of the feedwater hydrogen concentration. They showed that the effectiveness of this HWC depends strongly upon the location of the component in the primary coolant circuit. In response to the uncertain efficacy of HWC, noble-metal enhanced chemistry strategies (e.g., NOBLECHEM) have been devised [15–18], which involve the deposition of noble metals onto the steel surfaces. These deposits have the effect of catalyzing the hydrogen electrode reaction (probably preferentially over the oxygen and hydrogen peroxide electrode reactions), thereby rendering hydrogen a much more effective reducing agent than otherwise would be the case. The net result is the displacement of the ECP in the negative direction.

DAMAGE-PREDICTOR, ALERT, REMAIN, and FOCUS are evolutionary, deterministic codes developed by this group for predicting damage due to stress corrosion cracking in BWR primary coolant circuits as a function of the operating history of a plant. The codes are 'deterministic', because the outputs ('predictions') of the component models are constrained by known physicochemical laws. All of these codes, except REMAIN, are derivatives of the original code (DAMAGE-PREDICTOR) that was initially developed to model BWRs with external coolant pumps and internal jet pumps [9–13]. On the other hand, REMAIN was developed to predict IGSCC damage in German BWRs equipped with internal coolant pumps. DAMAGE-PREDICTOR was initially used to model two of the reactors (Duane Arnold and Dresden-2) that were included in the original study of Ruiz et al. [1], but has since been employed to model 14 operating BWRs worldwide. The ECP predictions provided by DAMAGE-PREDICTOR are, in general, similar to those obtained by Macdonald et al. [2] using the MPM and Ruiz et al.'s [1] calculated values for $[H_2]$, $[O_2]$, and $[H_2O_2]$.

A number of radiolysis codes have also been developed to calculate radiolytic species concentrations in PWR primary coolant circuits. These include codes by Christensen at Studsvik AB in Sweden [20], Dixon and coworkers at Atomic Energy of Canada Limited [21], and Burns and Moore at UKAEA [3]. All of the radiolysis codes confirm that the concentrations of the oxidizing radiolytic species (O_2, H_2O_2, OH) are low compared to those of various reducing species, such as H_2 and H, although differences do exist between the codes with respect to the actual values of the concentrations. However, none of these codes predicted the ECP, because they lacked a mixed potential model (MPM).

The ECP modeling work of Macdonald and coworkers [22–24] shows that under normal PWR primary circuit conditions [25 cc(STP)/kg] and in the absence of oxygen in the primary feedwater, the ECP is controlled primarily by the equilibrium potential of the hydrogen electrode reaction (HER) according to the following equation:

$$\mathrm{ECP} = -\left(\frac{2.303RT}{2F}\right)\log(f_{\mathrm{H_2}}) - \left(\frac{2.303RT}{F}\right)\mathrm{pH}_T, \tag{1}$$

where R is the universal gas constant, $f_{\mathrm{H_2}}$ is the fugacity (partial pressure) of hydrogen, F is Faraday's constant, and pH_T is the pH at the operating Kelvin temperature (T). ECP values calculated from Eq. (1), which assumes equilibrium, are of the order of -700 to -950 $\mathrm{mV_{SHE}}$, depending upon temperature, hydrogen concentration, and the concentrations of lithium and boron in the coolant (which determine the pH). This range of ECP is highly significant, in the light of the findings by Totsuka and Smialowska [25] that Alloy 600 in the mill-annealed condition suffers from hydrogen-induced cracking in alkaline solutions at potentials more negative than -800 $\mathrm{mV_{SHE}}$. Thus, on the basis of Totsuka and Smialowska's work, as noted by Macdonald and coworkers [23,26], Alloy 600 exists in a PWR primary coolant circuit operating with a high hydrogen concentration [>15 cc(STP)/kg] in a state of spontaneous intergranular fracture, due to HIC (hydrogen-induced cracking). Totsuka and Smialowska et al. [25] also observed stress corrosion cracking at potentials more positive than -650 $\mathrm{mV_{SHE}}$ in the same solution. Thus, for Alloy 600, at least, there exists a window of 150 mV over which the material is apparently immune to fracture. Macdonald et al. [23] used their radiolysis/ECP code to explore the impact of hydrogen concentration in displacing the ECP into the immune region (more positive ECPs). The hydrogen concentration so determined using the radiolysis/mixed potential code was about 5 cc(STP)/kg, assuming that no oxygen is added to the feedwater. The results of these calculations are encouraging, because

they suggest that ECP control may be a practical way of mitigating environmentally induced fracture in the primary coolant circuits of PWRs, in much the same way as is being achieved in BWRs. More recently, a comprehensive radiolysis/ECP code, PWR–ECP, has been developed for modeling PWR primary coolant circuits as a function of reactor operating parameters and coolant hydrogen concentration.

1.1. Theoretical basis

The main body of the code, PWR–ECP, is the water radiolysis model, which calculates the concentrations of radiolysis products from the decomposition of water due to neutron, gamma and alpha radiation. The water radiolysis model makes use of chemical reactions coupled to fluid convection, in order to calculate the concentrations of the species at points around the heat transport circuit. After the species concentrations have been determined, the ECP is then calculated using a mixed potential model (MPM). Incorporated into the MPM is the capability of: (i) exploring the impact of heterogeneous catalysis/inhibition of the redox reactions that occur on the metal surface, and (ii) incorporating various alloys, as the requisite electrochemical kinetic data for these reactions (oxidation of hydrogen and the reduction of oxygen and hydrogen peroxide) and the alloy electro-oxidation reactions becomes available. As of now, a reasonably complete set of data currently exists only for Type 304 SS. Auxiliary input parameters (such as flow velocity, coolant temperature, alpha, neutron, and gamma dose rates in the coolant) have been obtained from the International Atomic Energy Agency (IAEA) [28] and from running other available thermal hydraulic and dose rate codes. The regions covered by the model in a PWR heat transport circuit correspond to a hypothetical average PWR reactor with four loops, where only one loop is simulated. The pH and ECP were calculated around the primary coolant loop under normal full power operating conditions and under cold shut down conditions. Only the results obtained for the core and the steam generator will be discussed, due to restrictions on the length of this paper.

1.2. Water radiolysis

The radiolysis of water in PWR primary heat transport circuits has long been recognized as a potential source of corrosive, oxidizing species, such as O_2, H_2O_2, OH, etc. [3,23,27]. For this reason, hydrogen is added to suppress their radiolytic generation. However, in order to calculate the ECP, it is important that the concentrations of the most prevalent radiolytic species, at least, be determined, since the contributions that any given species makes to the corrosion potential is roughly proportional to its concentration. In order to calculate the species concentrations, the combined effects of the radiolytic yield of each species, due to radiation, and the changes in concentration due to chemical reactions and fluid convection must be taken into account. The impact of the radiolysis products is to displace the potential from the value calculated using Eq. (1), which assumes equilibrium conditions.

1.3. Chemical reactions

The chemical reactions occurring in the primary heat transport circuits of PWRs essentially determine the species concentrations in each part of the circuit, particularly in regions of low dose rate (i.e., in out-of-core regions). The general reaction set used in this study is given in Table 1, along with the rate constants and the activation energies.

The rate of change for each species i, at a given location c, R_i^c, is given by reaction rate theory as

$$R_i^c = \sum_{j=1}^{N} \sum_{m,s=1}^{M} k_j C_s C_m - C_i \sum_{j=1}^{N} \sum_{s=1}^{M} k_j C_s, \tag{2}$$

where k_j is the rate constant for the reaction between species s and m, or for the reaction between species s and i, and C_m, and C_s are the concentrations of species m and s, respectively. N is the number of reactions in the model (i.e., $N = 34$ (from Table 1)), M is the maximum number of species considered (i.e., $M = 14$ in this model).

The rate constant, k_j (j denotes the reaction number in Table 1), is a function of coolant temperature. Since the temperature throughout the heat transport circuit is not constant, the actual rate constant for each chemical reaction must be calculated for each specific position using Arrhenius' law:

$$k_j = k_0 \exp\left[\frac{E_a}{R}\left(\frac{1}{T_0} - \frac{1}{T_j}\right)\right], \tag{3}$$

where k_0 is the rate constant at temperature T_0 (the reference temperature), E_a is the activation energy (Table 1), R is the universal gas constant, and T

Table 1
Extended list of reactions considered in the water radiolysis model

No.	Rate constant (L/mol s)	Activation energy (kcal/mol)	Chemical reactions
1	1.6E+1	3.0	$e^- + H_2O = H + OH^-$
2	2.4E+10	3.0	$e^- + H^+ = H$
3	2.4E+10	3.0	$e^- + OH = OH^-$
4	1.3E+10	3.0	$e^- + H_2O_2 = OH + OH^-$
5	1.0E+10	3.0	$H + H = H_2$
6	2.0E+10	3.0	$e^- + HO_2 = HO_2^-$
7	1.9E+10	3.0	$e^- + O_2 = O_2^-$
8	5.0E+9	3.0	$2e^- + 2H_2O = 2OH^- + H_2$
9	4.5E+9	3.0	$OH + OH = H_2O_2$
10	1.2E+10	3.0	$OH + HO_2 = H_2O + O_2$
11	1.2E+10	3.0	$OH + O_2^- = OH^- + O_2$
12	2.0E+7	3.0	$OH^- + H = e^- + H_2O$
13	4.5E+8	3.0	$e^- + H + H_2O = OH^- + H_2$
14	6.3E+7	3.0	$e^- + HO_2^- + H_2O = OH + 2OH^-$
15	1.44E+11	3.0	$H^+ + OH^- = H_2O$
16	2.6E−5	3.0	$H_2O = H^+ + OH^-$
17	2.0E+10	3.0	$H + OH = H_2O$
18	3.4E+7	4.6	$OH + H_2 = H + H_2O$
19	2.70E+7	3.4	$OH + H_2O_2 = H_2O + HO_2$
20	4.4E+7	4.5	$H + H_2O_2 = OH + H_2O$
21	1.9E+10	3.0	$H + O_2 = HO_2$
22	8.0E+5	3.0	$HO_2 = O_2^- + H^+$
23	5.0E+10	3.0	$O_2^- + H^+ = HO_2$
24	2.7E+6	4.5	$2HO_2 = H_2O_2 + O_2$
25	1.7E+7	4.5	$2O_2^- + 2H_2O = H_2O_2 + O_2 + 2OH^-$
26	2.0E+10	3.0	$H + HO_2 = H_2O_2$
27	2.0E+10	3.0	$H + O_2^- = HO_2^-$
28	1.8E+8	4.5	$e^- + O_2^- + H_2\,sO = HO_2^- + OH^-$
29	1.8E+8	4.5	$OH^- + H_2O_2 = HO_2^- + H_2O$
30	1.9973E−6	14.8	$2H_2O_2 = 2H_2O + O_2$
31	1.04E−4	3.0	$H + H_2O = H_2 + OH$
32	1.02E+4	3.0	$H_2O + HO_2^- = H_2O_2 + OH^-$
33	1.5E+7	4.5	$HO_2 + O_2^- = O_2 + HO_2^-$
34	7.7E−4	7.3	$H_2O_2 = 2OH$

The rate constants were measured at 25 °C; and a temperature adjustment was performed in each reaction via Eq. (3). The rate constants and activation energies for Reactions 1–34 were used by Macdonald and coworkers [13] to model BWRs (the rate constant for Reaction 30 was used to calibrate the model to measure in-plant ECP data). All but the italic numbers were traced to the original publication of Burns and Moore [3]. The italicized numbers sources are Lukashenko [31] and Pastina [32].

is the operating temperature in Kelvin. The rate constant for hydrogen peroxide decomposition (Reaction No. 30) was calculated separately using an experimentally derived relationship [9]:

$$k_{30} = 1.4096 * 10^5 \cdot e^{-\left(\frac{14\,800}{RT}\right)}. \quad (4)$$

Notice that $[H^+]$ and $[OH^-]$ are calculated from the pH and the dissociation constant of water at the prevailing temperature.

1.4. Radiolytic yield

The rate at which any primary radiolytic species is produced is given by [9]

$$R_i^y = \left(\frac{G_i^\gamma \Gamma^\gamma}{100} + \frac{G_i^n \Gamma^n}{100} + \frac{G_i^\alpha \Gamma^\alpha}{100}\right)\widetilde{F}\rho/N_v, \quad (5)$$

where R_i^y has units of mol/cm^3 s, G^n, G^g, and G^α are the radiolytic yields for neutrons, gamma photons, and alpha particles, respectively, in number of particles per 100 eV of energy absorbed, N_v is Avogadro's number, $\widetilde{F}$ equals 6.25×10^{13} (the conversion factor from rad/s to eV/g s), and ρ is the water density in g/cm^3. Γ^γ, Γ^n, and Γ^α are the gamma photon, neutron, and alpha particle energy dose rates, respectively, in units of rad/s. Alpha particles are produced by the $^{10}B_5(^1n_0, ^4He_2)^7Li_3$ reaction and may make a significant contribution to the total

Table 2
G values for primary radiolytic species at high temperatures ('high: reported at high temperatures')

No.	Gamma [26] 285 °C	Radiolytic yields neutron [31] 285 °C	Alpha [27] 270–300 °C	Species
1	4.15	0.93	0.13	e^-
2	1.08	0.50	0.12	H
3	3.97	1.09	0.45	OH
4	1.25	0.99	1.55	H_2O_2
5	0.00	0.04	0.00	HO_2
6	0.00	0.00	0.00	HO_2^-
7	0.00	0.00	0.00	O_2
8	0.00	0.00	0.00	O_2^-
9	0.00	0.00	0.00	$O_2^{=}$
10	0.00	0.00	0.00	O^-
11	0.00	0.00	0.00	O
12	0.62	0.88	1.65	H_2
13	0.00	0.00	0.00	OH^-
14	4.15	0.93	0.13	H^+

radiolytic yield (>10%), depending upon the location.

Table 2 lists the radiolytic yields reported for aqueous solutions at roughly reactor operating temperatures. The species to which those values correspond are in the rightmost column. For comparison, Table 3 summarizes the radiolytic yields measured at a lower (ambient) temperature. Clearly, temperature exerts an important influence over the radiolytic yield.

1.5. Overall equations

By adopting the rates of change of species concentration from the various sources discussed above, we write the total rate of species formed by the effect of radiolysis as [9,24]

$$R_i = \left(\frac{G_i^{\gamma}\Gamma^{\gamma}}{100N_{\mathrm{v}}} + \frac{G_i^{\mathrm{n}}\Gamma^{\mathrm{n}}}{100N_{\mathrm{v}}} + \frac{G_i^{\alpha}\Gamma^{\alpha}}{100N_{\mathrm{v}}}\right)\widetilde{F}\rho + \left[\sum_{j=1}^{N}\sum_{m,s=1}^{M} k_j C_s C_m - C_i \sum_{j=1}^{N}\sum_{s=1}^{M} k_j C_s\right]. \quad (6)$$

The approach used in this work to solve the set of coupled ordinary differential equations (ODEs) makes use of a publicly available subroutine (DVODE), developed by Hindmarsh at the Lawrence Livermore National Laboratory in California. This algorithm is designed to solve first order, stiff ODE equation sets. Our system of equations is indeed coupled throughout via the concentrations of all the species considered (up to 14, depending of the case considered) and is very stiff.

The flux of each dissolved species is given by [9,24]

$$\overline{N}_i = -z_i D_i (F/RT) C_i \overline{\nabla}\phi - D_i \overline{\nabla} C_i + C_i \overline{V}, \quad \text{Flux} = \text{migration} + \text{diffusion} + \text{convection}, \quad (7)$$

where D_i is diffusivity of the redox species i, $\overline{N}_i$ is the vector flux of each dissolved species, z_i is the charge number (with sign) on the ion, R is the gas constant, T is the temperature, C_i and $\overline{\nabla} C_i$ are the species concentrations and concentration gradient; $\overline{\nabla}\phi$ is the electric field strength, F is Faraday's number, and $\overline{V}$ is the fluid velocity vector for each section considered. Note that velocity is considered in one dimension and is assumed to be constant in each unbranched section of uniform cross-sectional area.

Because of efficient mixing and in the absence of an electric field, we may ignore diffusion and migration, respectively, and hence, the material balance can be written as

$$\frac{\partial C_i}{\partial t} = -\overline{\nabla}\cdot\overline{N}_i + R_i, \quad (8)$$

(accumulation = net input + production) where R_i is the rate of production of the species in the fluid due to homogeneous reactions. Accordingly,

$$\frac{\partial C_i}{\partial t} = -\overline{\nabla}\cdot(C_i\overline{V}) + R = -C_i\frac{\partial V}{\partial x} - V\frac{\partial C_i}{\partial x} + R_i, \quad (9)$$

where V the velocity for each considered section, as noted above.

Table 3
G values for primary radiolytic species at low temperature ('low: reported at room temperatures')

No.	Gamma [16] 20 °C	Radiolytic yields due to: neutron [20] 20 °C	Alpha [20] 20 °C	Species
1	2.66	0.37	0.04	e^-
2	0.55	0.36	0.16	H
3	2.67	0.46	0.10	OH
4	0.72	1.00	1.3	H_2O_2
5	0.00	0.17	0.30	HO_2
6	0.00	0.00	0.00	HO_2^-
7	0.00	0.00	0.00	O_2
8	0.00	0.00	0.00	O_2^-
9	0.00	0.00	0.00	O^-
10	0.00	0.00	0.00	O
11	0.00	0.00	0.00	$O_2^{=}$
12	0.45	1.20	1.70	H_2
13	0.10	0.00	0.00	OH^-
14	2.76	0.37	0.04	H^+

1.6. Mixed potential model

After the concentration of each radiolysis species is calculated, the corrosion potential of the component can be calculated using a mixed potential model (MPM) [28]. The MPM is based on the physical condition that charge conservation must be obeyed at a corroding interface. Because electrochemical reactions transfer charge across a metal/solution interface at rates measured by the partial currents, the following equation expresses the charge conservation constraint:

$$\sum_{j=1}^{n} i_{\mathrm{R/O},j}(E) + i_{\mathrm{corr}}(E) = 0, \tag{10}$$

where $i_{\mathrm{R/O},j}$ is the partial current density due to the jth redox couple in the system and i_{corr} is the metal oxidation (corrosion) current density. These partial currents depend on the potential drop across the metal/solution interface.

In the current version of the MPM, developed for modeling the ECP of Type 304 SS in BWR primary circuits, the steel oxidation current density, i_{corr}, was modeled as an empirical function of voltage, based on the data of Lee [29],

$$i_{\mathrm{corr}} = \frac{e^{\frac{(E-E_o)}{b_f}} - e^{-\frac{(E-E_o)}{b_r}}}{384.62e^{\frac{4416}{T}} + X}, \tag{11}$$

where

$$X = \frac{e^{\frac{(E-E_o)}{b_f}}}{2.61 \times 10^{-3} e^{-\frac{4416}{T+0.523(E-E_o)^{0.5}}}} \tag{12}$$

and

$$E_o = 0.122 - 1.5286 * 10^{-3}\, T. \tag{13}$$

In these expressions, E is the voltage, E_o is an empirical constant that is derived from the polarization curve for the oxidation of the steel, and, b_f and b_r are the forward and reverse Tafel constants, respectively, for the metal dissolution reaction, with values of 0.06 V being assumed for both. In actual fact, they are empirical constants that were assumed *a priori* in fitting Eq. (11) to the current/voltage data. It is important to note that Eq. (11) applies strictly to Type 304 SS in near neutral solutions [29] and, hence, this expression may not be a good empirical model for stainless steels in PWR primary circuits. More recently, the authors have developed the point defect model [30] for the oxidation of a passive metal. This model yields the passive current density in the form

$$i_{\mathrm{corr}} = a * \exp(bE) + c, \tag{14}$$

where the parameters a, b, and c are given in terms of fundamental parameters, as described in the original publication [30]. The first term on the right side of Eq. (14) arises from the transmission of cations (via cation vacancies) across the passive film from the metal/film interface to the film/solution interface, while the second term reflects the transmission of oxygen ions (via oxygen vacancies) and/or metal interstitials in the reverse direction. We hoped to fit Eq. (14) to available experimental data from the literature for the alloys of interest (Alloy 600 and stainless steels, data for which are now being assessed) under the conditions that most closely approximate those that are present in the primary coolant circuits of PWRs. However, the required steady state current/voltage data is unavailable at the present time and this approach, which is more soundly based on the theory of passivity, had to be abandoned.

Because electrochemical kinetic data are available only for the hydrogen electrode reaction (HER, H_2/H^+), the oxygen electrode reaction (OER, O_2/H_2O), and the hydrogen peroxide electrode reaction (HPER, H_2O_2/H_2O), only H_2, O_2, and H_2O_2 can be considered as the redox species in the MPM. Fig. 1 shows the approximate metal alloy composition of a schematic representation of a PWR. In this paper, we did not differentiate between metal alloys, because the requisite data are not yet available. However, the model has the capability of accommodating those values as they are produced.

In solving Eq. (10) for potential (ECP), it is necessary to first express the redox current for each conjugate redox pair in terms of the potential and kinetic, thermodynamic, and mass transport parameters for the reaction. From electrochemical kinetic theory, The current density ($i_{\mathrm{R/O}}$) for a redox couple (e.g., O_2/H_2O, H^+/H_2, H_2O_2/H_2O)

$$\mathrm{R} \Longleftrightarrow \mathrm{O} + \mathrm{ne}, \tag{15}$$

(where R is the reduced species and O is the oxidized species) can be expressed in terms of a the generalized Butler–Volmer equation as

$$i_{\mathrm{R/O}} = \frac{e^{\frac{(E-E^e_{\mathrm{R/O}})}{b_a}} - e^{-\frac{(E-E^e_{\mathrm{R/O}})}{b_c}}}{\frac{1}{i_{0,\mathrm{R/O}}} + \frac{1}{i_{i,f}} e^{\frac{(E-E^e_{\mathrm{R/O}})}{b_a}} - \frac{1}{i_{i,\gamma}} e^{-\frac{(E-E^e_{\mathrm{R/O}})}{b_c}}}, \tag{16}$$

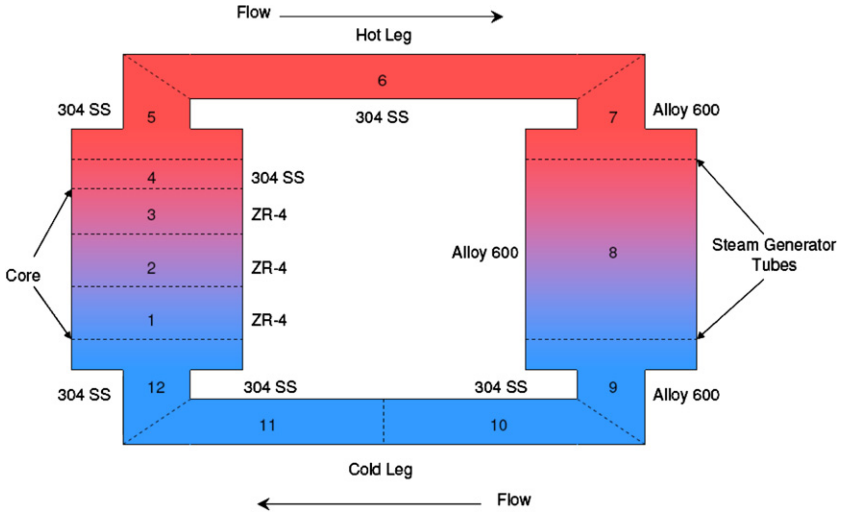

Fig. 1. Schematic of a PWR primary coolant circuit showing regions of different metallurgy.

where $i_{0,R/O}$ is the exchange current density, $i_{l,f}$ and $i_{l,r}$ are the mass-transfer limited currents for the forward and reverse directions of the redox reaction, respectively, and b_a and b_c are the anodic and cathodic Tafel constants. $E^e_{R/O}$ is the equilibrium potential for this reaction, as computed from the Nernst equation:

$$E^e_{R/O} = E^0_{R/O} - \frac{2.303RT}{nF}\log\left(\frac{a_R}{a_O}\right), \tag{17}$$

where a_R and a_O are the thermodynamic activities of R and O, respectively, and $E^0_{R/O}$ is the standard potential. Limiting currents are calculated using the equation [29]

$$i_{i,R/O} = \frac{\pm 0.0165 nFD_i C^b_{R/O} Re^{0.86} Sc^{0.33}}{d}. \tag{18}$$

The sign in Eq. (18) depends on whether the reaction occurs in the forward (+) or reverse (−) direction, F is Faraday's number, D_i is the diffusivity of the redox species, i, $C^b_{R/O}$ is the bulk concentration of R or O, as appropriate, Re is the Reynolds number ($Re = Vd/\eta$), Sc is the Schmidt number ($Sc = \eta/D_i$), d is the channel diameter, V is the flow velocity, n is electron number for the half cell reaction , and η is the kinematics viscosity.

1.7. Parameters values used in the calculation

The following parameters were adopted in these calculations:

$[O_2]$ = as indicated
$[H_2]$ = as indicated
Hydrodynamic diameters and flow velocities depend on the section considered
[Boron] = 840 mg/kg
[Lithium] = 1.9 mg/kg
Core bypass, gamma dose rate = $0.717 * 10^{+3}$ R/s
neutron dose rate = $1.29 * 10^{+3}$ R/s
alpha dose rate = $0.792 * 10^{+2}$ R/s
Outside of the core temperature range = 293–328 °C
Core temperature = 328 °C
Core radiation levels,
gamma dose rate = $0.286 * 10^{+6}$ R/s
neutrons dose rate = $0.514 * 10^{+6}$ R/s
alpha dose rate = $0.317 * 10^{+5}$ R/s

We explored two scenarios. In the first scenario, the oxygen concentration in the feedwater was maintained at zero and H_2 was injected into the primary circuit at the pressurizer. In the other, we maintained the H_2 concentration constant and changed the concentration of oxygen dissolved in the feedwater. We calculated the ECP around the primary loop of a PWR using the 'High' and 'Low' radiolytic yields and the set of reactions used by Macdonald and coworkers to model BWRs.

1.8. Experimental data

Fig. 2 shows a collection of experimental data for the ECP of stainless steels (Types 304 and 316)

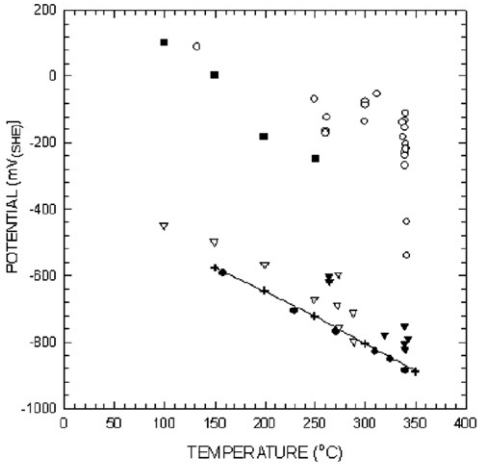

--+-- Calculated for 500 ppm B and 2 ppm Li at 350 °C with 2.8 ppm H_2
∘ Experimental data for 2.8 ppm H_2 at 300 °C
o Experiemntal data for 20-100 ppb residual O_2
∀ Data of Indig [19], for a "de-oxygenated" solution
▼ Experimental data for "de-oxygenated" solution
● Data of Lee [29], 0.001 to 0.1 Sodium Sulfate and approximated 100 ppb O_2

Fig. 2. Comparison of calculated electrochemical potentials for Type 304 and 316 SS with experimental data obtained in hydrogenated solutions and deoxygenated solutions [23].

obtained as a function of temperature (at temperatures up to PWR core conditions) in aqueous solutions containing various amounts of hydrogen and oxygen [23]. These data shows the strong effect expected when as little as 20 ppb of oxygen contaminates the feed water. The figure also shows that a corrosion potential (ECP) of about −700 to $-800\ mV_{SHE}$, corresponding to the hydrogen electrode potential at very high temperatures and with no oxygen in the feed water, might be expected in the primary coolant circuit of a PWR, in good agreement with calculation (see below). However, the data also suggest that, if even only small concentrations of oxidizing species are produced by radiolysis or are added via the feedwater (e.g., O_2), the potential (ECP) may be significantly more positive than that calculated and measured for hydrogenated solutions.

2. Results and discussion

During normal operation of a PWR, and with hydrogen concentrations that are sufficiently large to completely suppress the radiolytic generation of oxidizing species, such as oxygen and hydrogen peroxide, we can expect that the ECP in the core will closely follow that calculated for the hydrogen electrode. It is also expected that, for very high H_2 concentrations injected into the feed water of the reactor, the core will adopt a potential between -0.8 and $-0.9\ V_{SHE}$. If the hydrogen concentration is lowered, and the radiolytic generation of oxidizing species is allowed to occur, the ECP will shift in the positive direction, particularly at lower temperatures (the pump side of the steam generator, for example) [23]. Oxygen in the feedwater also has an impact on the ECP, because it shifts the electrochemical potential in the positive direction and, in extreme cases, may raise the ECP to the point where certain alloys, such as Alloy 600, may suffer stress corrosion cracking. Because the region of potential over which Alloy 600 is immune to either HIC (at $ECP < -800\ mV_{SHE}$) or SCC ($ECP > -650\ mV_{SHE}$) is so narrow (150 mV), it is evident that potential control in a PWR primary circuit will require a great deal of finesse.

Fig. 3 shows the predicted ECP throughout the primary loop of a PWR under normal operation. A constant H_2 concentration of 25 cc(STP)/kg, was assumed, while the O_2 concentration injected into the feedwater was varied. Note that increasing the O_2 concentration is predicted to increases the ECP. These calculations were performed by assuming the 34 reactions with 14 species adopted by Macdonald and coworkers for BWR simulation (Table 1) and the 'High' radiolytic yield set (Table 2). The hot parts of the core and the cold leg entrance to the core display ECP values that are approximately the same as the hydrogen electrode reactions.

Fig. 4 shows the predicted ECP throughout the primary loop of a PWR for the same conditions assumed in Fig. 3, except that the 'Low' set of radiolytic yields (Table 3) was assumed. Note that, again, increasing the O_2 concentration increases the ECP. It is evident, however, that the calculated potential versus distance around the primary coolant circuit is sensitive to the set of data assumed for the yields of radiolytic species, particularly in the core, hot-leg, steam generator, and cold-leg regions. At the current time, we do not know which of the two radiolytic data sets are more realistic. This question could only be answered by measuring the ECP in the circuit; unfortunately these data are not currently available. Thus, the importance of employing an accurate set of radiolytic yield data is well demonstrated.

The calculated data plotted in Fig. 5 shows the ECP in the primary loop of a PWR at constant O_2 concentration (5 ppb O_2) and as a function of

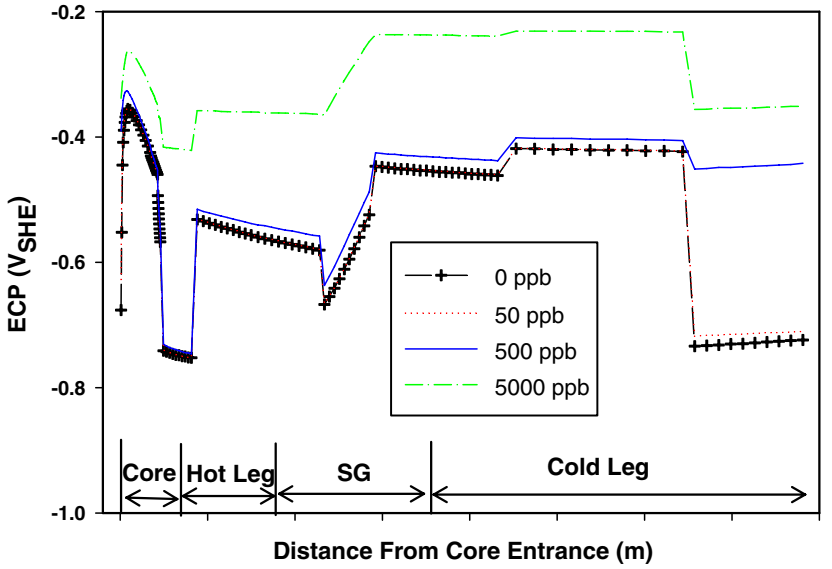

Fig. 3. Calculated ECP throughout the primary loop of a PWR. The O_2 concentration injected into the feedwater was varied from 0 ppb to 5000 ppb. The H_2 was maintained constant at 25 cc(STP)/kg. The 'High' radiolytic yield set (Table 2) was used in the calculations.

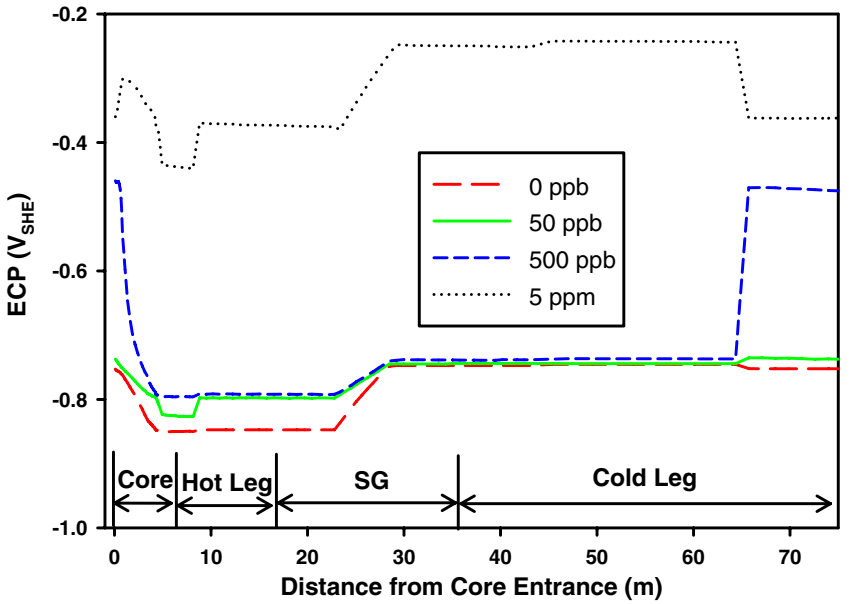

Fig. 4. Calculated ECP throughout the primary loop of a PWR. The O_2 concentration injected into the feedwater was varied. The H_2 was maintained constant at 25 cc(STP)/kg. The 'Low' radiolytic yield set was used in the calculations.

the H_2 concentration. The calculations employed the 'High' set of radiolytic yields. The results of the calculations indicate that even if $[H_2] = 35$ cc(STP)/kg, as little as 5 ppb of oxygen injected into the feedwater, will have a significant impact on displacing the ECP in the positive direction (compare Figs. 5 and 3).

Fig. 6 shows the predicted ECP in the primary loop of a PWR at constant O_2 concentration (5 ppb O_2) as a function of the specified H_2 concentration [1–35 cc(STP)/kg]. The calculations employed the 'Low' set of radiolytic yields. By adopting this set of radiolytic yields, the calculated ECP is predicted to remain at very negative values

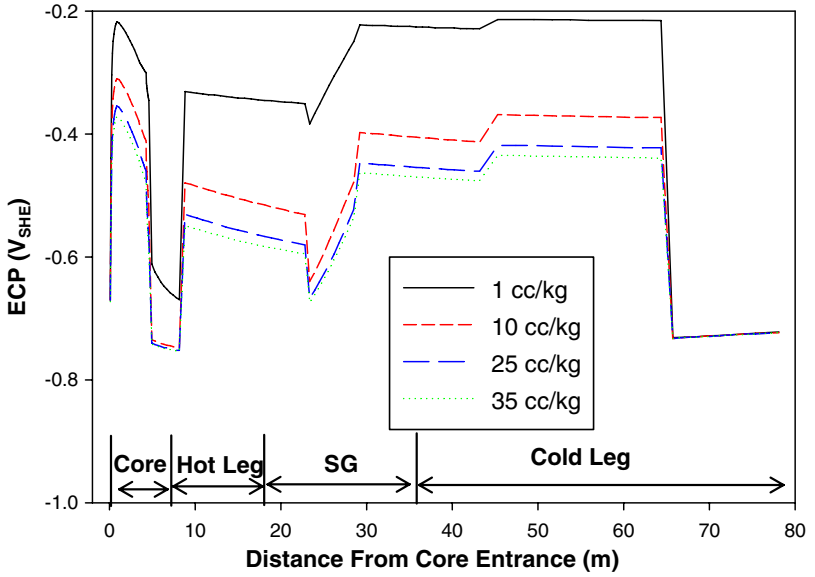

Fig. 5. Calculated ECP in the primary loop of a PWR. Constant O_2 concentration is 5 ppb and H_2 concentration was varied as indicated. The model uses the 'High' set of radiolytic yields.

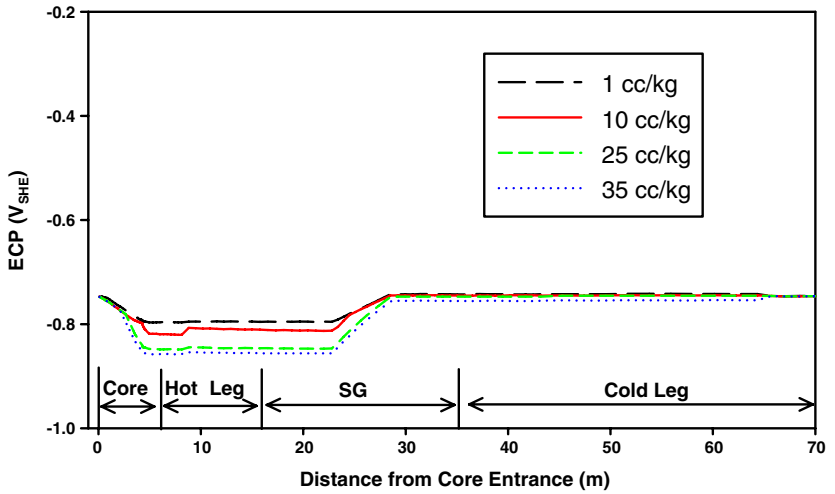

Fig. 6. Calculated ECP in the primary loop of a PWR. The O_2 concentration is 5 ppb and H_2 concentration was varied as indicated. The model uses the 'Low' set of radiolytic yields.

(at the hydrogen electrode potential), even in the case where there was 5 ppb of oxygen in the feedwater of the primary reactor loop. Again, these calculations demonstrate the high sensitivity of the predicted ECP to the values assumed for the radiolytic yields, as concluded above.

Experimental measurements (Fig. 2) appear to indicate that twenty ppb levels of dissolved oxygen in the coolant reactor loop will shift the ECP of the primary loop (at temperatures between 250 and 350 °C) to an area of potential where stress corrosion cracking occurs (ECP $> -650\ mV_{SHE}$ for Alloy 600). Calculation of the ECP, by adopting the 34 reactions used by Macdonald and coworkers in BWRs and the radiolytic yields measured at 'high' temperatures (see Table 2), show that the corrosion potential is very sensitive to oxygen contamination. The results also show that a part of the core has a calculated ECP greater than $-400\ mV_{SHE}$ when operating with sufficient hydrogen to

'suppress radiolysis'. Clearly, the divergent results discussed in this paper argue for the development of more reliable and accurate data sets for the radiolytic yield for various species produced by the radiolysis of water under PWR primary coolant circuit operating conditions.

3. Conclusion and recommendations

At this point, it is important to determine how accurate the radiolysis model needs to be in predicting the concentrations of radiolytic species. Bearing in mind that, if our objective is to calculate the ECP, it is evident from the mixed potential model that the contribution that any given species makes to determining the corrosion potential is roughly proportional to its concentration. Thus, only those electro-active species that are present at the highest concentrations will have a significant impact on the ECP. These species include (as determined from previous modeling of BWR primary circuits [9]): H_2 (added to the coolant), possibly O_2 (feedwater component), H_2O_2, e^- (aq), and OH (radiolysis), with the latter two being of doubtful significance. If oxygen is not a component of the feedwater, its predicted concentration in a hydrogenated PWR coolant is virtually zero (in our calculations zero concentration are assigned to any species with a concentration below 10^{-12} M level). Thus, the important question is whether O_2 can survive the passage through the core at a concentration that is not significantly reduced from the feedwater value. *The essential requirement is, therefore, that the model accurately predicts the concentrations of the most abundant species, not that it predicts the concentrations of all species accurately.* We believe the proposed model meets these requirements, but that the results that are obtained are very sensitive to the radiolytic yield data that are assumed in the calculation. It is therefore essential that accurate data be determined for the yields under the operating conditions of the reactor.

Acknowledgments

The authors gratefully acknowledge the support of this work by the US Department of Energy through the Nuclear Energy Education Research (NEER) program via Grant No. DE-FG07-02ID14334.

References

[1] C.P. Ruiz, et al., Modeling hydrogen water chemistry for BWR applications, EPRI NP-6386, Electric Power Research Institute, June 1989.
[2] D.D. Macdonald et al., in: Proceedings of the International Conference on Chemistry in Water Reactors: Operating Experience and New Developments, Nice, France, April 24–27, 1994.
[3] W.G. Burns, P.B. Moore, Radiat. Eff. 30 (1976) 233.
[4] M.L. Lukashenko et al., Atom. Energy. 72 (1992) 570.
[5] C.C. Lin et al., Int. J. Chem. Kinet. 23 (1991) 971.
[6] E. Ibe et al., J. Nucl. Sci. Technol. 23 (1986) 11.
[7] J. Chun, Modeling of BWR Water Chemistry, Master Thesis, Department of Nuclear Engineering, Massachusetts Institute of Technology, 1990.
[8] D.D. Macdonald, M. Urquidi-Macdonald, Corrosion 46 (1990) 380.
[9] T.-K. Yeh, D.D. Macdonald, A.T. Motta, Nucl. Sci. Eng. 121 (1995) 468.
[10] T.-K. Yeh, D.D. Macdonald, A.T. Motta, Nucl. Sci. Eng. 123 (1996) 295.
[11] T.-K. Yeh, D.D. Macdonald, A.T. Motta, Nucl. Sci. Eng. 123 (1996) 305.
[12] D.D. Macdonald, M. Urquidi-Macdonald, Corrosion 52 (1996) 659.
[13] T.-K. Yeh, C.-H. Liang, M.-S. Yu, D.D. Macdonald, in: Proc. 8th Int. Symp. Environ. Degrad. Mater. Nucl. Power Sys. Water Reactors, Amelia Island, GA, August 1995.
[14] D.D. Macdonald, I. Balachov, G. Engelhardt, Power Plant Chem. 1 (1) (1999) 9.
[15] L.W. Niedrach, Corrosion 47 (1991) 162.
[16] Y-J. Kim, P.L. Andressen, D.M. Gray, Y-C. Lau, H.P. Offer, Corrosion 52 (1996) 40.
[17] Y-J. Kim, L.W. Niedrach, P.L. Andressen, Corrosion 52 (1996) 738.
[18] P.L. Andresen, Y.-J. Kim, T.P. Diaz, S. Hettiarachchi, in: Proc. 12th Int. Conf. Environ. Degrad. Mater. Nucl. Power Sys. Water Reactors, August 14–18 2005, Salt Lake City, UT, Minerals, Metals and Materials Society, TMS; American Nuclear Society, ANS; NACE International, 2005, p. 727.
[19] M. Indig, L. Nelson, Corrosion 47 (1991) 202.
[20] H. Christensen, Nucl. Technol. 109 (1995) 373.
[21] E.L. Rosinger, R.S. Dixon, AECL Report 5958, 1977.
[22] A. Bertuch, D.D. Macdonald, J. Pang, L. Kriksunov, K. Arioka, in: Proc. 6th Int. Symp. Environ. Degrad. Mater, Nucl. Power Sys. Water Reactor, San Diego, CA, NACE International, August 1–5, 1993, p. 905.
[23] A. Bertuch, J. Pang, D.D. Macdonald, in: Proc. 7th Int. Symp. Environ. Degrad. Mater. Nucl. Power Sys. Water Reactors, NACE International, Houston, TX, 2, 1995, p. 687.
[24] D. Macdonald, M.U. Macdonald, J. Mahaffy, A. Jain, Electrochemistry of water-cooled nuclear reactors, Unpublished Report to DOE, 2003.
[25] N. Totsuka, Z. Szklarska-Smialowska, Corrosion 43 (1987) 734.
[26] D.D. Macdonald, in: 7th Int. Symp. Environ. Degrad. Nucl. Power Sys. Reactors, 1995, p. 687.
[27] W.G. Burns, J. Henshaw, J.A.B. Goodball, The radiation chemistry of a pressurized water reactor, The effect of added

hydrogen based on a simplified modeling approach, AEA Technology, Report AEA RS 3478, July 1994.
[28] D.D. Macdonald, Corrosion 48 (1992) 194.
[29] J.B. Lee, Electrochemical approach to corrosion problems of several iron–nickel–chromium alloys in high temperature, high pressure water, PhD Dissertation, Ohio State University, Columbus, OH, 1978.
[30] D.D. Macdonald, J. Electrochem. Soc. 139 (1992) 3434.
[31] M.L. Lukashenko, Atom. Energy 72 (6) (1992) 570.
[32] L.B. Pastina, J. Nucl. Mater. 264 (1999) 309.